

DARK MATTER: WHAT, HOW AND WHERE?*

Y. MAMBRINI

Laboratoire de Physique Théorique, Université Paris-Sud
91405 Orsay, France*(Received June 7, 2010)*

Dark Matter experiments reached an incredible range of sensitivities these last years. They are now able to probe large regions of parameter space of the more popular extensions of the Standard Model (MSSM, KK modes, extra dark forces). They even become competitive with LHC discovery prospects. We try in this presentation to summarize the specific characteristics of the most favored candidates (what?), the theoretical difficulties inherent to the calculation of their different detection rates (how?) and the uncertainties related to their presence in our galaxy (where?).

PACS numbers: 11.30.Pb, 98.62.Gq, 98.80.Ft, 95.35.+d

1. Introduction

From the quoted contributions to Ω in matter and baryons from WMAP, we can obtain the density of cold Dark Matter from the difference between the total matter density and the baryon density [1]

$$\Omega_{\text{CDM}}h^2 = 0.1099 \pm 0.0062 \quad (1.1)$$

or a 2σ range of 0.0975–0.1223 for $\Omega_{\text{CDM}}h^2$.

Evidence for Dark Matter in the Universe is available from a wide range of observational data. In addition to the results from the CMB, there is the classic evidence from galactic rotation curves [2], which indicate that nearly all spiral galaxies are embedded in a large galactic halo of Dark Matter leading to rather constant rotational velocities at large distances from the center of the galaxy (in contrast to the expected $v^2 \sim 1/r$ behavior in the absence of Dark Matter). Other dramatic pieces of evidence can be found in combinations of X-ray observations and weak lensing showing the superposition of Dark Matter (from lensing) and ordinary matter from

* Presented at the Cracow Epiphany Conference on Physics in Underground Laboratories and Its Connection with LHC, Cracow, Poland, January 5–8, 2010.

X-ray gas [3] and from the separation of baryonic and Dark Matter after the collision of two galaxies as seen in the Bullet cluster [4]. For a more complete discussion see [5].

In addition to being stable (or at least very long lived), the Dark Matter should be both electrically and color neutral. Indeed, there are very strong constraints, forbidding the existence of stable or long lived particles which are not color and electrically neutral as these would become bound with normal matter forming anomalously heavy isotopes. The limits on the abundances, relative to hydrogen, of nuclear isotopes [6], $n/n_H \lesssim 10^{-15}$ to 10^{-29} for $1 \text{ GeV} \lesssim m \lesssim 1 \text{ TeV}$. A strongly interacting stable relic is expected to have an abundance $n/n_H \lesssim 10^{-10}$ with a higher abundance for charged particles.

Unfortunately, there are no viable candidates for Dark Matter in the Standard Model. As baryons and neutrinos have been excluded, one is forced to go beyond the Standard Model, and here, I will focus on the possibilities which exist in the context of the minimal supersymmetric extension of the Standard Model (MSSM) [7]. In the MSSM, the lightest supersymmetric particle (LSP) is stable if R-parity ($R = -1^{3B+L+2s}$) is unbroken. There are several possibilities in the MSSM, specifically the sneutrino with spin zero, the neutralino with spin 1/2, and the gravitino with spin 3/2. However, a sneutrino LSP would have relatively large coherent interactions with heavy nuclei, and experiments searching directly for the scattering of massive Dark Matter particles on nuclei exclude a stable sneutrino weighing between a few GeV and several TeV [8]. The possible loophole of a very light sneutrino was excluded by measurements of the invisible Z -boson decay rate at LEP [9]. The gravitino is a viable candidate and often predicted in models based on supergravity [10, 11]. In this case, however, its probability for direct detection is negligible.

2. What: The Dark Matter in the Universe

Several candidates appeared to conciliate WMAP data within the framework of Standard Model extensions: extra-gauge bosons, extra-dimension modes, scalar Dark Matter. But the most promising extension is the supersymmetric one which gives to the theoretician two valid candidates, the neutralino and gravitino. We will review here each of their characteristics.

2.1. Neutralino Dark Matter

The Standard Model (SM) of high-energy physics, despite of its success in explaining the data available today, requires an extension to explain the stability of the hierarchy between the weak and the Planck scales, the unification of gauge couplings and the origin of electroweak symmetry breaking.

The most plebiscite extension of the model is the Minimal Supersymmetric Standard Model (MSSM) [12–15]. It predicts the existence of several new particles, the superpartners of SM ones. The lightest supersymmetric particle (LSP) is in most of the MSSM parameter space, a stable, massive, neutral and weakly interacting particle: the lightest neutralino, which is thus an interesting and well motivated Dark Matter candidate. On the other hand, at future colliders such as the Large Hadron Collider (LHC) and the planned International Linear e^+e^- Collider (ILC), supersymmetric particles are expected to be produced and observed if low energy Supersymmetry (SUSY) is present in nature. However, even if part of the supersymmetric spectrum is unveiled at the LHC for example, the properties of the particles which play a dominant role in the relic density will not be measured directly or precisely. Both types of data (from astroparticle and accelerator physics) are thus needed to extract more complete properties of the underlying supersymmetric model [16].

The four neutralinos ($\chi_1^0 \equiv \chi, \chi_2^0, \chi_3^0, \chi_4^0$) are superpositions of the neutral fermionic partners of the electroweak gauge bosons \tilde{B}^0 and \tilde{W}_3^0 (respectively the B -ino and W -ino fields) and the superpartners of the neutral Higgs bosons $\tilde{H}_u^0, \tilde{H}_d^0$ (respectively up and down Higgsinos fields). In the $(\tilde{B}, \tilde{W}^3, \tilde{H}_d^0, \tilde{H}_u^0)$ basis, the neutralino mass matrix is given by

$$\mathcal{M}_N = \begin{pmatrix} M_1 & 0 & -m_Z \cos \beta \sin \theta_W & m_Z \sin \beta \sin \theta_W \\ 0 & M_2 & m_Z \cos \beta \cos \theta_W & -m_Z \sin \beta \cos \theta_W \\ -m_Z \cos \beta \sin \theta_W & m_Z \cos \beta \cos \theta_W & 0 & -\mu \\ m_Z \sin \beta \sin \theta_W & -m_Z \sin \beta \cos \theta_W & -\mu & 0 \end{pmatrix}, \quad (2.2)$$

where M_1, M_2 are the bino and wino mass parameters, respectively. This matrix can be diagonalized by a single orthogonal matrix z and we can express the LSP χ (often referred in the following as *the neutralino*) as

$$\chi = z_{11} \tilde{B} + z_{12} \tilde{W} + z_{13} \tilde{H}_d + z_{14} \tilde{H}_u. \quad (2.3)$$

This combination determines the nature, the couplings and the phenomenology of the neutralino. The neutralino is usually called “gaugino-like” if $P \equiv |z_{11}|^2 + |z_{12}|^2 > 0.9$, “Higgsino-like” if $P < 0.1$, and “mixed” otherwise.

Depending on the nature of the neutralino, the WMAP constraint can be fulfilled essentially by bino- $\chi\tilde{\tau}$ coannihilation processes if $m_\chi \sim m_{\tilde{\tau}_1}$, $\chi\chi \xrightarrow{A} b\bar{b}$ annihilation for large $\tan\beta$ values or a light pseudoscalar A boson, and $\chi\chi \rightarrow t\bar{t}$ for a sufficiently Higgsino-like neutralino. At the same time, a non negligible wino component can enhance the annihilation process $\chi\chi \rightarrow W^+W^-$ and the $\chi\chi^\pm$ and $\chi^+\chi^-$ coannihilation ones (see Fig. 1).

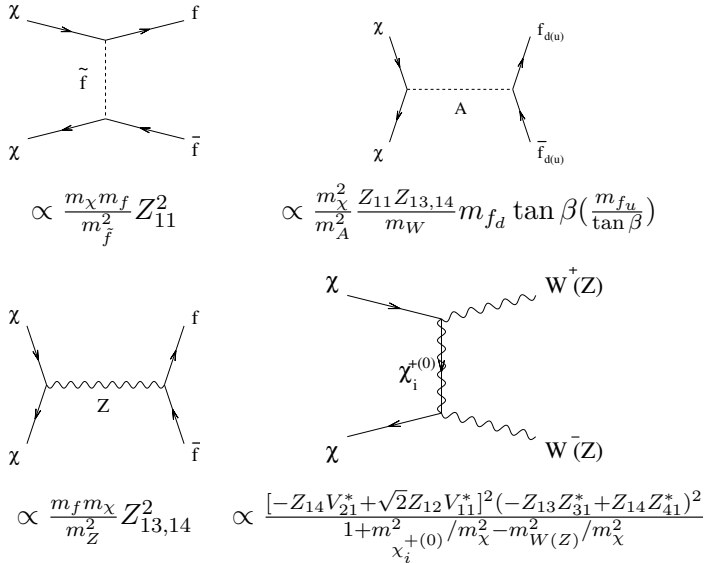


Fig. 1. Dominant neutralino annihilation diagrams. Relevant parts of the amplitudes are shown explicitly. Terms between parenthesis correspond to f_u and Z final states in second and fourth diagrams. V and Z are chargino and neutralino mixing matrices.

2.2. The gravitino Dark Matter

In scenarios with gravitino Dark Matter, the late decay of the Next to Lightest Supersymmetric Particle (NLSP) into the LSP produces electromagnetic and hadronic showers. If the decay takes place after Big Bang Nucleosynthesis (BBN), the products of these showers may alter the primordial abundances of light elements [18]. Also, the late injection of electromagnetic energy may distort the frequency dependence of the cosmic microwave background spectrum from its observed blackbody shape [19–21].

It has been shown that hadronic BBN constraints rule out the possibility of neutralino NLSP for gravitino masses above $m_{3/2} \gtrsim 100$ MeV [22–25]. However, if the NLSP is the lightest stau $\tilde{\tau}_1$ we should also take into account bound-states effects on the primordial ${}^6\text{Li}$ abundance. Indeed, it has been shown [26] that bound-state formation of $\tilde{\tau}_1^-$ with ${}^4\text{He}$ can lead to an overproduction of ${}^6\text{Li}$ via the catalyzed BBN (CBBN) reaction ${}^4\text{He} X^- + \text{D} \rightarrow {}^6\text{Li} + X^-$ [27]. Thus, the observationally inferred upper limit on the primordial ${}^6\text{Li}$ abundance [28] implies a stringent upper bound on the stau NLSP lifetime

$$\tau_{\tilde{\tau}_1} \lesssim 5 \times 10^3 \text{ s.} \quad (2.4)$$

A similar bound can be extracted using the same arguments to avoid overproduction of ${}^9\text{Be}$ (see, *e.g.*, [29, 30]). In the case of a stau NLSP decays, the stau decays primarily to the gravitino and a τ lepton at tree level, via gravitational interactions with a lifetime [31, 32]

$$\tau_{\tilde{\tau}_1} \simeq \Gamma^{-1}(\tilde{\tau}_1 \rightarrow \tilde{G}\tau) = 6.1 \times 10^6 \left(\frac{m_{\tilde{G}}}{100 \text{ GeV}}\right)^2 \left(\frac{100 \text{ GeV}}{m_{\tilde{\tau}}}\right)^5 \left(1 - \frac{m_{\tilde{G}}^2}{m_{\tilde{\tau}}^2}\right)^{-4} \text{ s}. \quad (2.5)$$

The relic abundance of gravitinos receives contributions from two different sources. First, there is a non-thermal production (NTP) of gravitinos in the late decays of the NLSP. Since each NLSP decays into one gravitino, the non-thermal relic abundance of the latter is related to that of the NLSP [33, 34]

$$\Omega_{\tilde{G}}^{\text{NTP}} h^2 = \frac{m_{3/2}}{m_{\text{NLSP}}} \Omega_{\text{NLSP}}^{\text{TP}} h^2 \sim 0.02 \left(\frac{m_{3/2}}{100 \text{ GeV}}\right) \left(\frac{m_{\text{NLSP}}}{1 \text{ TeV}}\right). \quad (2.6)$$

Second, gravitinos are also thermally produced (TP) through scatterings in the plasma, the resulting relic abundance being proportional to the reheating temperature T_{R} of the Universe after inflation [35, 36]

$$\Omega_{\tilde{G}}^{\text{TP}} h^2 \simeq 0.32 \left(\frac{100 \text{ GeV}}{m_{3/2}}\right) \left(\frac{m_{\tilde{g}}}{1 \text{ TeV}}\right)^2 \left(\frac{T_{\text{R}}}{10^7 \text{ GeV}}\right). \quad (2.7)$$

The total relic density is the sum of both contributions $\Omega_{\tilde{G}} h^2 = \Omega_{\tilde{G}}^{\text{NTP}} h^2 + \Omega_{\tilde{G}}^{\text{TP}} h^2$, to which we apply the constraint extracted from the WMAP data [37]. The model studied in [38] is a nice example of mixed scenario with mixed gravitino/neutralino Dark Matter.

3. How: Detection of the Dark Matter candidate

3.1. Direct detection

In spite of the experimental challenges, a number of efforts worldwide are actively pursuing to directly detect WIMPs with a variety of targets and approaches. Many direct Dark Matter detection experiments are now either operating or in preparation. All these experiments measure the number N of elastic collisions between WIMPs and target nuclei in a detector, per unit detector mass and per unit of time, as a function of the nuclear recoil energy E_{r} . The detection rate in a detector depends on the density $\rho_0 \simeq 0.3 \text{ GeV cm}^{-3}$ and velocity distribution $f(v_{\chi})$ of WIMPs near the Earth. In general, the differential event rate per unit detector mass and per

unit of time can be written as:

$$\frac{dN}{dE_r} = \frac{\sigma_{\chi-N} \rho_0}{2 m_r^2 m_\chi} F(E_r)^2 \int_{v_{\min}(E_r)}^{\infty} \frac{f(v_\chi)}{v_\chi} dv_\chi, \quad (3.8)$$

where the WIMP-nucleus cross-section, $\sigma_{\chi-N}$, is related to the WIMP-nucleon cross-section, $\sigma_{\chi-p}$, by $\sigma_{\chi-N} = \sigma_{\chi-p} (Am_r/M_r)^2$, with $M_r = \frac{m_\chi m_p}{m_\chi + m_p}$ the WIMP-nucleon reduced mass, $m_r = \frac{m_\chi m_N}{m_\chi + m_N}$ the WIMP-nucleus reduced mass, m_χ the WIMP mass, m_N the nucleus mass, and A the atomic weight. F is the form factor.

For the velocity distribution we take a simple Maxwellian halo

$$f(v_\chi) d^3v_\chi = \frac{1}{(v_\chi^0)^3 \pi^{3/2}} e^{-(v_\chi/v_\chi^0)^2} d^3v_\chi, \quad (3.9)$$

where $v_\chi^0 = 220 \pm 20$ km/s is the velocity of the Sun around the galactic center with its uncertainty, and we have neglected the motion of the Earth around the Sun. After integrating over the angular part in order to find the speed distribution we get:

$$f(v_\chi) dv_\chi = \frac{4 v_\chi^2}{(v_\chi^0)^3 \sqrt{\pi}} e^{-(v_\chi/v_\chi^0)^2} dv_\chi. \quad (3.10)$$

The integration over velocities is limited to those which can give place to a recoil energy E_r , thus there is a minimal velocity given by $v_{\min}(E_r) = \sqrt{\frac{m_N E_r}{2 m_r^2}}$.

The effective interaction between the WIMP and a nucleus is given by the Woods–Saxon form factor

$$F(E_r) = \frac{3 j_1(q R_1)}{q R_1} e^{-(qs)^2}, \quad (3.11)$$

where the transferred momentum is $q = \sqrt{2 m_N E_r}$, j_1 is a spherical, first-order Bessel function, $R_1 = \sqrt{R^2 - 5 s^2}$ with $R \simeq 1.2 A^{1/3}$ fm, A is the mass number, and $s \simeq 1$ fm.

In Fig. 2 we show an example of a signal with a standard neutron background in a XENON-like (100 kg) experiment, after 3 years of data acquisition, as a function of the recoil energy. For a WIMP mass of 100 GeV and a WIMP-nucleon cross-section of 10^{-9} pb, such an experiment would reach a pretty large χ^2 per degree of freedom (χ_{red}^2), of the order of 60.

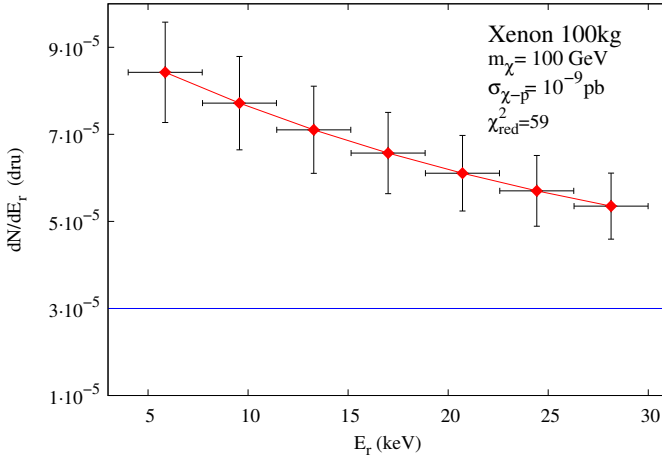


Fig. 2. XENON event rate expectations for the case of differential rate *versus* recoil energy of the nucleus for a WIMP mass $m_\chi = 100$ GeV and cross-section $\sigma_{\chi-p} = 10^{-9}$ pb. The error bars shown are those expected for the XENON 100 kg experiment after 3 years of observation. The lower (blue) line is the background-only prediction. The χ^2 per degree of freedom (χ^2_{red}) is 59, giving a signal clearly distinguishable from the background.

3.2. Indirect detection of gamma-rays

The spectrum of gamma-rays generated in Dark Matter annihilations and coming from a direction forming an angle ψ with respect to the galactic center is

$$\Phi_\gamma(E_\gamma, \psi) = \sum_i \frac{dN_\gamma^i}{dE_\gamma} Br_i \langle \sigma v \rangle \frac{1}{8\pi m_\chi^2} \int_{\text{line of sight}} \rho^2 dl, \quad (3.12)$$

where the discrete sum is over all Dark Matter annihilation channels, dN_γ^i/dE_γ is the differential gamma-ray yield, $\langle \sigma v \rangle$ is the annihilation cross-section averaged over its velocity distribution, Br_i is the branching ratio of annihilation into final state i , and ρ is the Dark Matter density.

It is customary to rewrite Eq. (3.12) introducing the dimensionless quantity J (which depends only on the Dark Matter distribution):

$$J(\psi) = \frac{1}{8.5 \text{ kpc}} \left(\frac{1}{0.3 \text{ GeV/cm}^3} \right)^2 \int_{\text{line of sight}} \rho^2(r(l, \psi)) dl. \quad (3.13)$$

After having averaged over a solid angle, $\Delta\Omega$, the gamma-ray flux can now be expressed as

$$\Phi_\gamma(E_\gamma) = 0.94 \times 10^{-13} \text{ cm}^{-2} \text{ s}^{-1} \text{ GeV}^{-1} \text{ sr}^{-1} \\ \times \sum_i \frac{dN_\gamma^i}{dE_\gamma} \left(\frac{Br_i \langle \sigma v \rangle}{10^{-29} \text{ cm}^3 \text{ s}^{-1}} \right) \left(\frac{100 \text{ GeV}}{m_\chi} \right)^2 \bar{J}(\Delta\Omega) \Delta\Omega. \quad (3.14)$$

The value of $\bar{J}(\Delta\Omega)\Delta\Omega$ depends crucially on the Dark Matter distribution. The most common parametrization of the different profiles that have been proposed in the literature is

$$\rho(r) = \frac{\rho_0 [1 + (R_0/a)^\alpha]^{(\beta-\gamma)/\alpha}}{(r/R_0)^\gamma [1 + (r/a)^\alpha]^{(\beta-\gamma)/\alpha}}, \quad (3.15)$$

where ρ_0 is the local (solar neighborhood) halo density, a is a characteristic length, and R_0 the distance from the Sun to the galactic center. As mentioned above, we use $\rho_0 = 0.3 \text{ GeV/cm}^3$, but recent analysis [39] showed that a factor 2 of uncertainty exists on its precise determination.

N -body simulations suggest a cuspy inner region of Dark Matter halo with a distribution where γ generally lies in the range 1 (NFW profile [40]) to 1.5 (Moore *et al.* profile [41]), producing a profile with a behavior $\rho(r) \propto r^{-\gamma}$ at small distances. Over a solid angle of $4 \times 10^{-3} \text{ sr}$, such profiles can lead from $\bar{J}(\Delta\Omega) \sim 5.859 \times 10^2$ to 2.574×10^4 . Moreover, if we take into account the baryon distribution in the Galaxy, we can predict even more cuspy profiles with γ in the range 1.45 to 1.65 ($\bar{J}(\Delta\Omega) \sim 3.254 \times 10^4 - 3.075 \times 10^5$) through the adiabatic compression process (see the study of Refs. [42, 43]). We summarize the parameters used in our study and the values of \bar{J} for each profile in Table I. The calculation is obviously not altered whatever DM candidate is assumed and is therefore valid for an arbitrary WIMP. A monochromatic line can also be generated by DM annihilation and observed at FERMI telescope [45].

TABLE I

NFW and Moore *et al.* density profiles without and with adiabatic compression (NFW_c and Moore_c, respectively) with the corresponding parameters, and values of $\bar{J}(\Delta\Omega)$.

	a (kpc)	α	β	γ	$\bar{J}(4 \times 10^{-3} \text{ sr})$
NFW	20	1	3	1	5.859×10^2
NFW _c	20	0.8	2.7	1.45	3.254×10^4
Moore <i>et al.</i>	28	1.5	3	1.5	2.574×10^4
Moore _c	28	0.8	2.7	1.65	3.075×10^5

3.3. Indirect detection of antiprotons

Antiprotons can be produced either by Dark Matter annihilations or through different kinds of astrophysical mechanisms. After being produced they propagate in the Galaxy and reach the Earth, where they can be detected as exotic components in cosmic rays. The PAMELA experiment reported recently [46] the measurement of the antiproton to proton flux ratio up to 100 GeV, which is in agreement with that predicted by the conventional background model. In the near future, the AMS-02 experiment, to be launched next year, will measure the antiproton flux with even higher precision, increasing the odds of finding an additional component due to Dark Matter annihilations.

3.3.1. Propagation

Once produced, antiprotons propagate throughout the galaxy undergoing several processes:

- They scatter on irregularities of the galactic magnetic field — Alfvén waves. These scatterings constitute, in fact, a space diffusion process with a diffusion coefficient given by

$$K(E_{\text{kin}}) = K_0 \beta_{\bar{p}} \left(\frac{p_{\bar{p}}}{\text{GeV}} \right)^\delta, \quad (3.16)$$

where E_{kin} is the antiproton kinetic energy, $p_{\bar{p}} = (E_{\text{kin}}^2 + 2m_{\bar{p}}E_{\text{kin}})^{1/2}$ is the antiproton momentum, and $\beta_{\bar{p}} = \left(1 - \frac{m_{\bar{p}}^2}{(E_{\text{kin}} + m_{\bar{p}})^2} \right)^{1/2}$. K_0 and δ are free parameters of the propagation model that are constrained by a combination of theoretical predictions and astrophysical data.

- They undergo a second order Fermi mechanism reacceleration, due to the motion of the scattering centers with a velocity of $V_a \approx (20-100) \frac{\text{km}}{\text{s}}$. This reacceleration process is described by the coefficient

$$K_{EE} = \frac{2}{9} V_a^2 \frac{E^2 \beta^4}{K(E)}. \quad (3.17)$$

- They lose energy either adiabatically, or through Coulomb scattering, or by ionizing the interstellar (IS) medium. The total energy loss rate is denoted by b and depends on the antiproton energy.
- They are wiped away from the galactic disk through convection, with a velocity $V_c \approx (5-15) \frac{\text{km}}{\text{s}}$. In the following, this velocity will be taken to be completely vertical to the disk: $V_c = V_c \text{sign}(z)$.

- They can annihilate upon scattering on the IS medium. In this study, we shall consider the two primary components of the medium, namely Hydrogen and Helium. The annihilation cross-sections for \bar{p} -H and \bar{p} -He scattering have been taken from [47], where the well-known Tan&Ng parametrization [48] is used.

The propagation of antiprotons in the interstellar medium, taking into account all of the above processes, is described by a diffusion-convection equation of the form

$$\partial_z(V_c\psi) - K\nabla\psi + \partial_E[b(E)\psi - K_{EE}(E)\partial_E\psi] = q, \quad (3.18)$$

where we denote by $\psi = dn/dE$ the energy density of the antiprotons, and by q the source term — see equation (3.22). Actually, this equation is rather generic and can be applied to other particles species propagating in the galaxy. Only the values of the different parameters, but not the equation itself, will vary depending on the propagating particle. We will see in Section 3.4, for instance, that this same equation describes the propagation of positrons in the interstellar medium. Let us now see how to solve this equation for antiprotons.

3.3.2. The primary flux

To solve equation (3.18), we shall use the method proposed, for example, in [49, 50, 53]. The idea of this method is to adopt a simpler version of equation (3.18) for which the Green function can be calculated analytically. To achieve such simplification, certain processes contributing to the final antiproton spectrum have to be neglected. Specifically, all energy redistributions in the initial (injection) spectrum — energy losses, reacceleration, as well as “tertiary” contributions (*i.e.* contributions from secondary antiprotons produced upon inelastic scattering with the IS medium) — are ignored. Whether these redistributions are important or not depends mainly on the antiproton energy. For GeV energies, the results may deviate up to 50% from those obtained with the (more complete) Bessel function treatment — in [54] a comparison between the two methods can be found (see Fig. 2). But for energies around 10 GeV, the accuracy of the method improves dramatically, yielding essentially indistinguishable results at slightly higher energies. Since the \bar{p} energy region we shall consider begins at 10 GeV, we can safely use this simplified approach. Apart from its clearer physical interpretation, the main advantage of this method is that astrophysical effects can be separated from particle physics ones. As a result, it is a well-suited method for scans in parameter spaces, as those we are going to carry out in the following.

If we denote by $\Gamma_{\bar{p}}^{\text{ann}} = \sum_{\text{ISM}} n_{\text{ISM}} v \sigma_{\bar{p} \text{ ISM}}^{\text{ann}}$ the destruction rate of antiprotons in the ISM, where ISM = H, He, and implementing the aforementioned simplifications, the transport equation for a point source (which actually defines the propagator G) is:

$$\left[-K \nabla + V_c \frac{\partial}{\partial z} + 2h \Gamma_{\text{tot}} \delta(z) \right] G = \delta(\vec{r} - \vec{r}'). \quad (3.19)$$

The antiproton propagator can then be written as

$$G_{\bar{p}}^{\odot}(r, z) = \frac{e^{-k_v z}}{2\pi K L} \sum_{n=0}^{\infty} c_n^{-1} K_0(r \sqrt{k_n^2 + k_v^2}) \sin(k_n L) \sin(k_n(L - z)), \quad (3.20)$$

where K_0 is a modified Bessel function of the second kind and

$$\begin{aligned} c_n &= 1 - \frac{\sin(k_n L) \cos(k_n L)}{k_n L}, \\ k_v &= V_c / (2K), \\ k_d &= 2h \Gamma_{\bar{p}}^{\text{ann}} / K + 2k_v, \end{aligned} \quad (3.21)$$

with $h = 100$ pc being the half thickness of the galactic disc, and L being the half-thickness of the diffusive zone. k_n is obtained as the solution of the equation

$$n\pi - k_n L - \arctan(2k_n/k_d) = 0, \quad n \in \mathbb{N}.$$

Then, in order to compute the flux expected on earth, we should convolute the Green function (3.20) with the source distribution $q(\vec{r}, E)$. For Dark Matter annihilations in the galactic halo, the source term is given by

$$q(\vec{r}, E) = \frac{1}{2} \left(\frac{\rho(\vec{x})}{m_\chi} \right)^2 \sum_i \left(\langle \sigma v \rangle \frac{dN_{\bar{p}}^i}{dE_{\bar{p}}} \right), \quad (3.22)$$

where the index i runs over all possible annihilation final states. The decay of SM particles into antiprotons can be calculated with programs like PYTHIA [57]. In the singlet scalar model of Dark Matter, antiprotons may originate in W^\pm , Z^0 , h , and t decays. Regarding the distribution of Dark Matter in the Galaxy, $\rho(\vec{x})$, we assume a NFW profile with a local density of 0.3 GeV cm^3 . The final expression for the antiproton flux on the Earth takes the form

$$\Phi_{\odot}^{\bar{p}}(E_{\text{kin}}) = \frac{c\beta}{4\pi} \frac{\langle \sigma v \rangle}{2} \left(\frac{\rho(\vec{x}_{\odot})}{m_\chi} \right)^2 \frac{dN}{dE}(E_{\text{kin}}) \int_{DZ} \left(\frac{\rho(\vec{x}_s)}{\rho(\vec{x}_{\odot})} \right)^2 G_{\bar{p}}^{\odot}(\vec{x}_s) d^3x, \quad (3.23)$$

where none of the integrated quantities depends on the antiproton energy. This feature demonstrates one of the virtues of the Green function method applied to antiprotons: The integral in equation (3.23), which we compute using a VEGAS Monte-Carlo algorithm, needs to be calculated only once for each value of the injection energy, for it is the same as the detection energy.

Regarding the propagation parameters L , K_0 , δ , and V_c , we take their values from the well-established MIN, MAX and MED models — see Table II. The former two models correspond to the minimal and maximal antiprotons fluxes that are compatible with the B/C data. The MED model, on the other hand, correspond to the parameters that best fit the B/C data.

TABLE II

Values of propagation parameters widely used in the literature and providing minimal and maximal antiproton fluxes, or constitute the best fit to the B/C data.

	L (kpc)	K_0 (kpc ² /Myr)	δ	V_c (km/s)
MIN	1	0.0016	0.85	13.5
MED	4	0.0112	0.70	12.0
MAX	15	0.0765	0.46	5.0

3.3.3. Influence of substructures

N -body simulations reveal that galactic halos are not completely smooth; they also contain a significant number of substructures (clumps). Such substructures have been studied repeatedly in the literature as a possible way to enhance the Dark Matter annihilation rate. It has been claimed though, that in realistic scenarios it is rather improbable to expect large enhancements from Dark Matter clumps [49]. Here, we will study rather qualitatively the possible effect of substructures on the antiproton (and positron) signal.

To that end, we closely follow the approach outlined in [50]. The enhancement due to Dark Matter substructure is described by an energy-dependent function known as the boost factor B . Because the distribution of Dark Matter clumps in the Galaxy is unknown, B cannot be computed from first principles; it can only be studied from a statistical point of view. For simplicity, we will limit our discussion to the effective boost factor, B_{eff} , defined as the average value of B over a large number of realizations of the Galactic halo. It must be kept in mind, however, that in some exceptional cases — for example when there is a large Dark Matter clump very close to the Earth — B_{eff} can deviate significantly from B . The probability of such an event is quite small [52].

The energy-dependent effective boost factor, B_{eff} , can be written, under certain assumptions (see [50]), as

$$B_{\text{eff}} \equiv \frac{\langle \phi \rangle}{\phi_{\text{sm}}} = (1 - f)^2 + f B_c \frac{\mathcal{I}_1}{\mathcal{I}_2}, \quad (3.24)$$

where $\langle \phi \rangle$ is the average flux coming from the clumpy DM distribution, ϕ_{sm} is the flux that we would expect if the whole halo were smooth, f is the fraction of DM in clumps, and B_c is the boost factor (assumed constant with energy) for an individual clump. In this study, this constant boost factor is supposed to be universal for all clumps. Finally, $\mathcal{I}_{n=1,2}$ are given by

$$\mathcal{I}_n = \int_{\text{DM halo}} G(\vec{x}, E) \left(\frac{\rho_{\text{sm}}(\vec{x})}{\rho_0} \right)^n d^3\vec{x}. \quad (3.25)$$

The effective boost factor, then, depends on f and B_c . When invoking clumpiness, we will follow [50] and use $f = 0.2$ as a representative value (see *e.g.* [55,56]). Regarding the constant boost factor, B_c , it could vary from just a few up to two orders of magnitude [49,51,56]. We will use $B_c = 3, 10, 100$, which give rise to effective boost factors in the approximate ranges (1, 2), (3, 5) and (10, 40) respectively. This last range roughly coincides with the upper limit for the boost factor found in [49], for the case of a NFW smooth halo and clumps with a Moore et al internal profile.

3.4. Indirect detection of positrons

We now discuss the positron signal from singlet Dark Matter annihilation, carrying out an analysis similar to that presented for antiprotons in the previous section.

3.4.1. Propagation

There have been many treatments on the propagation of positrons throughout the galactic medium. In this paper, we adopt the two-zone diffusion model and solution described in [50]. For completeness, we review here the main points of this approach.

Being a diffusive process, positron propagation is governed by the same general equation, (3.18), that describes antiproton propagation. The approximations and the parameters that were used for antiprotons, however, are not the same as for positrons. Indeed, contrary to the \bar{p} case, where energy redistribution processes become inefficient above a few GeV, energy loss — through either synchrotron radiation or inverse Compton scattering on stellar light and CMB photons — is the main process involved in positron

propagation. These processes lead to an energy loss rate that can be written as

$$b(E) = \frac{E^2}{E_0 \tau_E}, \quad (3.26)$$

where E is the positron energy, E_0 is a reference energy (which we take to be 1 GeV) and $\tau_E = 10^{16}$ s is the characteristic energy-loss time.

The other important difference with respect to antiprotons is that for positron propagation the effect of the galactic convective wind, as well as reacceleration and annihilation processes can all be neglected. After these simplifications are taken into account, we are left with the following equation

$$\partial_t \psi - \nabla [K(x, E) \nabla \psi] - \partial_E [b(E) \psi] = q(x, E), \quad (3.27)$$

where K is the space diffusion coefficient — steady state is assumed. This coefficient is taken to be constant in space but depends on the energy as

$$K(E) = K_0 \left(\frac{E}{E_0} \right)^\alpha. \quad (3.28)$$

Here the diffusion constant, K_0 , and the spectral index, α , are propagation parameters. Then, the master equation for positron propagation gets simplified to its final form

$$K_0 \epsilon^\alpha \Delta \psi + \frac{\partial}{\partial \epsilon} \left(\frac{\epsilon^2}{\tau_E} \psi \right) + q = 0, \quad (3.29)$$

where $\epsilon = E/E_0$. This is the equation we solve to calculate the effects of positron propagation on a signal produced at some point in the galaxy.

As in the case of antiprotons, a crucial factor in the treatment of positron propagation is the adopted propagation model. In this case there are mainly 3 relevant parameters, namely L , K_0 and α ; that is, the half-thickness of the cylindrical diffusive zone, the diffusion constant and the spectral index, respectively. For their values we use the three models described in Table III.

TABLE III

Values of propagation parameters widely used in the literature and roughly providing minimal and maximal positron fluxes, or constitute the best fit to the B/C data.

	L (kpc)	K_0 (kpc ² /Myr)	α
MIN	1	0.00595	0.55
MED	4	0.0112	0.70
MAX	15	0.0765	0.46

3.4.2. The primary flux

The resulting positron flux from DM annihilations can be written as (see [60] for details)

$$\Phi_{e^+}(E) = \frac{\beta_{e^+} \langle \sigma v \rangle}{4\pi} \frac{1}{2} \left(\frac{\rho(\vec{x}_\odot)}{m_\chi} \right)^2 \frac{\tau_E}{E^2} \int_E^{m_\chi} f(E_s) \tilde{I}(\lambda_D) dE_s, \quad (3.30)$$

where the detection and the production energy are denoted respectively by E and E_s . $f(E_s)$ is the production spectrum for positrons, $f(E_s) = \sum_i dN_{e^+}^i/dE_s$, with i running over all possible annihilation channels. The diffusion length, λ_D , is defined by

$$\lambda_D^2 = 4K_0\tau_E \left(\frac{E^{\alpha-1} - E_s^{\alpha-1}}{1 - \alpha} \right). \quad (3.31)$$

The so-called halo function, \tilde{I} , contains all the dependence on astrophysical factors. It is given as

$$\tilde{I}(\lambda_D) = \int_{DZ} d^3\vec{x}_s \tilde{G}(\vec{x}_\odot, E \rightarrow \vec{x}_s, E_s) \left(\frac{\rho(\vec{x}_s)}{\rho(\vec{x}_\odot)} \right). \quad (3.32)$$

The modified Green function \tilde{G} is in its turn defined by

$$\tilde{G} = \frac{1}{4\pi K_0 \tilde{\tau}} e^{-(z_\odot - z_s)^2/4K_0\tilde{\tau}} \tilde{V}, \quad (3.33)$$

with \tilde{V} depending on the value of the characteristic parameter $\zeta = \frac{L^2}{K_0\tilde{\tau}}$. When $\zeta > 1$ — when the diffusion time is small — boundary conditions can be ignored and the propagation equation can be treated as a 1- D Schroedinger equation. In that case

$$\tilde{V} = \frac{1}{\sqrt{4\pi K_0 \tilde{\tau}}} \exp\left(-\frac{(z - z_s)^2}{4\pi K_0 \tilde{\tau}}\right). \quad (3.34)$$

When ζ is small this approximation no longer holds but we can express \tilde{V} as

$$\tilde{V} = \sum_{n=1}^{\infty} \frac{1}{L} \left[e^{-\lambda_n \tilde{\tau}} \phi_n(z_s) \phi_n(z) + e^{-\lambda'_n \tilde{\tau}} \phi'_n(z_s) \phi'_n(z) \right], \quad (3.35)$$

where

$$\phi_n(z) = \sin(k_n(L - |z|)), \quad k_n = \left(n - \frac{1}{2}\right) \frac{\pi}{L}, \quad (3.36)$$

$$\phi'_n(z) = \sin(k'_n(L - z)), \quad k'_n = n \frac{\pi}{L}. \quad (3.37)$$

An example of the influence of the propagation modes in the DM detection prospects can be found in [64], whereas a model independent complementary search between all these detections modes is analysed in [65].

4. Where: The halos models

A crucial ingredient for the calculation of the flux of gamma rays and antimatter propagation is the Dark Matter density profile of our galaxy. The different profiles that have been proposed in the literature can be parameterised as [66]

$$\rho(r) = \frac{\rho_0[1 + (R_0/a)^\alpha]^{(\beta-\gamma)/\alpha}}{(r/R_0)^\gamma[1 + (r/a)^\alpha]^{(\beta-\gamma)/\alpha}}, \quad (4.38)$$

where ρ_0 is the local (solar neighborhood) halo density and a is a characteristic length. Highly cusped profiles are deduced from N -body simulations¹. In particular, NFW [40] obtained a profile with a behaviour $\rho(r) \propto r^{-1}$ at small distances. A more singular behaviour, $\rho(r) \propto r^{-1.5}$, was obtained by Moore *et al.* [41]. However, these predictions are valid only for halos without baryons. One can improve simulations in a more realistic way by taking into account the effect of the normal gas (baryons). This loses its energy through radiative processes falling to the central region of forming galaxy. As a consequence of this redistribution of mass, the resulting gravitational potential is deeper, and the Dark Matter must move closer to the center increasing its density.

This increase in the Dark Matter density is often treated using adiabatic invariants. The present form of the adiabatic compression model was numerically and analytically studied by Blumental *et al.* [68]. This model assumes spherical symmetry, circular orbit for the particles, and conservation of the angular momentum $M(r)r = \text{const.}$, where $M(r)$ is the total mass enclosed within radius r . The mass distributions in the initial and final configurations are therefore related by $M_i(r_i)r_i = [M_b(r_f) + M_{\text{DM}}(r_f)]r_f$, where $M_i(r)$, $M_b(r)$ and $M_{\text{DM}}(r)$ are the mass profile of the galactic halo before the cooling of the baryons (obtained through N -body simulations), the baryonic composition of the Milky Way observed now, and the to be determined Dark Matter component of the halo today, respectively. This approximation was tested in numerical simulations [69, 70]. Nevertheless, a more precise approximation can be obtained including the possibility of elongated orbits [42]. In this case, the mass inside the orbit, $M(r)$, is smaller than the real mass, the one the particle ‘feels’ during its revolution around the galactic center. As a consequence, the modified compression model is based on the conservation

¹ For analytical derivations see *e.g.* the recent work [67], and references therein.

of the product $M(\bar{r})r$, where \bar{r} is the averaged radius of the orbit. The time average radii is given by $\bar{x} \sim 1.72x^{0.82}/(1 + 5x)^{0.085}$, with $x \equiv r/r_s$, and r_s the characteristic radius of the assumed approximation.

The results are summarized in Table IV. There we label the resulting NFW and Moore *et al.* profiles with adiabatic compression by NFW_c and Moore_c , respectively. As one can see, at small r the Dark Matter density profile following the adiabatic cooling of the baryonic fraction is a steep power law $\rho \propto r^{-\gamma_c}$ with $\gamma_c \approx 1.45(1.65)$ for a $\text{NFW}_c(\text{Moore}_c)$ compressed model². We observe for example that the effect of the adiabatic compression on a NFW profile is basically to transform it into a Moore *et al.* one (see Table IV). Let us remark that NFW and Moore *et al.* profiles can be considered as a lower and upper limit, respectively. For example, the one recently proposed by Diemand, Moore and Stadel in Ref. [71], where $\rho(r) \propto r^{-1.16}$, is between both ‘standard’ profiles. It is worth noticing than some mechanisms can be advocated to reduce the effect of the compression like angular momentum transfer to Dark Matter or formation of the central black hole by spiraling and merging of two black holes.

TABLE IV

NFW and Moore *et al.* density profiles without and with adiabatic compression (NFW_c and Moore_c respectively) with the corresponding parameters, and values of $\bar{J}(\Delta\Omega)$.

	a (kpc)	α	β	γ	$\bar{J}(10^{-3}\text{sr})$	$\bar{J}(10^{-5}\text{sr})$
NFW	20	1	3	1	1.214×10^3	1.264×10^4
NFW_c	20	0.8	2.7	1.45	1.755×10^5	1.205×10^7
Moore <i>et al.</i>	28	1.5	3	1.5	1.603×10^5	5.531×10^6
Moore_c	28	0.8	2.7	1.65	1.242×10^7	5.262×10^8

Of course, these results have important implications for the computation of the gamma-ray fluxes from the galactic center. In particular, in Table IV we see that for $\Delta\Omega = 10^{-3}$ sr one has $\bar{J}_{\text{NFW}_c}/\bar{J}_{\text{NFW}} \simeq 145$ and $\bar{J}_{\text{Moore}_c}/\bar{J}_{\text{Moore et al.}} \simeq 77$. Thus the effect of the adiabatic compression is very strong, increasing the gamma-ray fluxes about two orders of magnitude. Similarly, for $\Delta\Omega = 10^{-5}$ sr one obtains $\bar{J}_{\text{NFW}_c}/\bar{J}_{\text{NFW}} \simeq 953$ and $\bar{J}_{\text{Moore}_c}/\bar{J}_{\text{Moore et al.}} \simeq 95$. More refine treatments of Dark Matter annihilation effects in the innermost region of the galaxy can be found in [73, 74].

² It is worth noticing that we obtain the same order of magnitude as the authors of Ref. [73].

5. Conclusions

We saw in this mini-review how theoretically complicated can be the detection of Dark Matter. A lot of uncertainties still exist: from the N -body simulation for the indirect detection of gamma rays, to the quarks-components of the proton for the direct detection, and the propagation parameters of cosmic rays for the anti-matter signals. From the model building, the task is also difficult as we need to embed the local relic abundance of Dark Matter into a coherent thermal history of the the Universe where still a lot have to be understood. All these dark points push us forward to find the solution to such a fascinating puzzle.

Y. Mambriini wants to thank the organizer for having him discovered such a nice city as Kraków, and the nice and very competent community of Polish particle physicists. The work of Y. Mambriini is supported by the European Network MRTN-CT-2006-035505 and the French ANR TADPMS.

REFERENCES

- [1] J. Dunkley *et al.* [WMAP Collaboration], *Astrophys. J. Suppl.* **180**, 306 (2009) [[arXiv:0803.0586\[astro-ph\]](#)]; E. Komatsu *et al.* [WMAP Collaboration], *Astrophys. J. Suppl.* **180**, 330 (2009) [[arXiv:0803.0547\[astro-ph\]](#)].
- [2] S.M. Faber, J.J. Gallagher, *Annu. Rev. Astron. Astrophys.* **17**, 135 (1979); A. Bosma, *Ap. J.* **86**, 1825 (1981); V.C. Rubin, W.K. Ford, N. Thonnard, *Ap. J.* **238**, 471 (1980); V.C. Rubin, D. Burstein, W.K. Ford, N. Thonnard, *Ap. J.* **289**, 81 (1985); T.S. Van Albada, R. Sancisi, *Phil. Trans. R. Soc. Lond.* **A320**, 447 (1986); M. Persic, P. Salucci, *Ap. J. Suppl.* **99**, 501 (1995); M. Persic, P. Salucci, F. Stel, *Mon. Not. R. Astron. Soc.* **281**, 27P (1996).
- [3] D. Wittman *et al.*, *Astrophys. J.* **643**, 128 (2006) [[arXiv:astro-ph/0507606](#)].
- [4] D. Clowe *et al.*, *Astrophys. J.* **648**, L109 (2006) [[arXiv:astro-ph/0608407](#)].
- [5] K.A. Olive, [arXiv:astro-ph/0301505](#).
- [6] J. Rich, M. Spiro, J. Lloyd-Owen, *Phys. Rep.* **151**, 239 (1987); T. Yamagata, Y. Takamori, H. Utsunomiya, *Phys. Rev.* **D47**, 1231 (1993); T.K. Hemmick *et al.*, *Phys. Rev.* **D41**, 2074 (1990); P.F. Smith, *Contemp. Phys.* **29**, 159 (1998); D. Javorsek, D. Elmore, E. Fischbach, D. Granger, T. Miller, D. Oliver, V. Teplitz, *Phys. Rev.* **D65**, 072003 (2002).
- [7] P. Fayet, *Phys. Lett.* **B64**, 159 (1976); *Phys. Lett.* **B69**, 489 (1977); *Phys. Lett.* **B84**, 416 (1979); H.E. Haber, G.L. Kane, *Phys.Rep.* **117**, 75 (1985).
- [8] T. Falk, K.A. Olive, M. Srednicki, *Phys. Lett.* **B339**, 248 (1994) [[arXiv:hep-ph/9409270](#)]; C. Arina, N. Fornengo, *J. High Energy Phys.* **0711**, 029 (2007) [[arXiv:0709.4477\[hep-ph\]](#)].

- [9] LEP Collaborations, ALEPH, DELPHI, L3 and OPAL, LEP Electroweak Working Group, SLD Electroweak Group, SLD Heavy Flavor Group, [hep-ex/0312023](#).
- [10] J.R. Ellis, K.A. Olive, Y. Santoso, V.C. Spanos, *Phys. Lett.* **B573**, 162 (2003) [[arXiv:hep-ph/0305212](#)]; J.R. Ellis, K.A. Olive, Y. Santoso, V.C. Spanos, *Phys. Rev.* **D70**, 055005 (2004) [[arXiv:hep-ph/0405110](#)].
- [11] J.R. Ellis, K.A. Olive, Y. Santoso, V.C. Spanos, *Phys. Lett.* **B588**, 7 (2004) [[arXiv:hep-ph/0312262](#)]; J.L. Feng, A. Rajaraman, F. Takayama, *Phys. Rev. Lett.* **91**, 011302 (2003) [[arXiv:hep-ph/0302215](#)]; J.L. Feng, S. Su, F. Takayama, *Phys. Rev.* **D70**, 075019 (2004) [[arXiv:hep-ph/0404231](#)].
- [12] P. Fayet, S. Ferrara, *Phys. Rep.* **32**, 249 (1977).
- [13] H.E. Haber, G.L. Kane, *Phys. Rep.* **117**, 75 (1985).
- [14] R. Barbieri, *Riv. Nuovo Cim.* **11N4**, 1 (1988).
- [15] S.P. Martin, [arXiv:hep-ph/9709356](#).
- [16] B.C. Allanach, G. Belanger, F. Boudjema, A. Pukhov, *J. High Energy Phys.* **0412**, 020 (2004) [[arXiv:hep-ph/0410091](#)].
- [17] J. Pradler, F.D. Steffen, *Phys. Lett.* **B648**, 224 (2007) [[arXiv:hep-ph/0612291](#)]; K. Jedamzik, M. Lemoine, G. Moultaqa, *J. Cosm. Astropart. Phys.* **0607**, 010 (2006) [[arXiv:astro-ph/0508141](#)].
- [18] R.H. Cyburt, J.R. Ellis, B.D. Fields, K.A. Olive, *Phys. Rev.* **D67**, 103521 (2003) [[arXiv:astro-ph/0211258](#)]; M. Kawasaki, K. Kohri, T. Moroi, *Phys. Lett.* **B625**, 7 (2005) [[arXiv:astro-ph/0402490](#)]; M. Kawasaki, K. Kohri, T. Moroi, *Phys. Rev.* **D71**, 083502 (2005) [[arXiv:astro-ph/0408426](#)].
- [19] W. Hu, J. Silk, *Phys. Rev. Lett.* **70**, 2661 (1993).
- [20] J.R. Ellis, J.E. Kim, D.V. Nanopoulos, *Phys. Lett.* **B145**, 181 (1984).
- [21] K. Hagiwara *et al.* [Particle Data Group], *Phys. Rev.* **D66**, 010001 (2002).
- [22] J.L. Feng, S. Su, F. Takayama, *Phys. Rev.* **D70**, 075019 (2004) [[arXiv:hep-ph/0404231](#)].
- [23] L. Roszkowski, R. Ruiz de Austri, K.Y. Choi, *J. High Energy Phys.* **0508**, 080 (2005) [[arXiv:hep-ph/0408227](#)].
- [24] R.H. Cyburt, J.R. Ellis, B.D. Fields, K.A. Olive, V.C. Spanos, *J. Cosm. Astropart. Phys.* **0611**, 014 (2006) [[arXiv:astro-ph/0608562](#)].
- [25] D.G. Cerdeño, K. Y. Choi, K. Jedamzik, L. Roszkowski, R. Ruiz de Austri, *J. Cosm. Astropart. Phys.* **0606**, 005 (2006) [[arXiv:hep-ph/0509275](#)].
- [26] J. Pradler, F.D. Steffen, *Phys. Lett.* **B666**, 181 (2008) [[arXiv:0710.2213\[hep-ph\]](#)]; S. Bailly, K. Jedamzik, G. Moultaqa, *Phys. Rev.* **D80**, 063509 (2009) [[arXiv:0812.0788\[hep-ph\]](#)].
- [27] M. Pospelov, *Phys. Rev. Lett.* **98**, 231301 (2007) [[arXiv:hep-ph/0605215](#)]; M. Pospelov, J. Pradler, F.D. Steffen, *J. Cosm. Astropart. Phys.* **0811**, 020 (2008) [[arXiv:0807.4287\[hep-ph\]](#)].
- [28] R.H. Cyburt, J.R. Ellis, B.D. Fields, K.A. Olive, *Phys. Rev.* **D67**, 103521 (2003) [[arXiv:astro-ph/0211258](#)].

- [29] J. Pradler, F.D. Steffen, *Phys. Lett.* **B666**, 181 (2008) [arXiv:0710.2213[hep-ph]].
- [30] M. Pospelov, J. Pradler, F.D. Steffen, *J. Cosm. Astropart. Phys.* **0811**, 020 (2008) [arXiv:0807.4287[hep-ph]].
- [31] J.L. Feng, S. Su, F. Takayama, *Phys. Rev.* **D70**, 075019 (2004) [arXiv:hep-ph/0404231].
- [32] J.R. Ellis, K.A. Olive, Y. Santoso, V.C. Spanos, *Phys. Lett.* **B588**, 7 (2004) [arXiv:hep-ph/0312262].
- [33] S. Borgani, A. Masiero, M. Yamaguchi, *Phys. Lett.* **B386**, 189 (1996) [arXiv:hep-ph/9605222]; T. Asaka, K. Hamaguchi, K. Suzuki, *Phys. Lett.* **B490**, 136 (2000) [arXiv:hep-ph/0005136]; J.L. Feng, A. Rajaraman, F. Takayama, *Phys. Rev. Lett.* **91**, 011302 (2003) [arXiv:hep-ph/0302215].
- [34] F.D. Steffen, arXiv:0711.1240[hep-ph]; *AIP Conf. Proc.* **903**, 595 (2007) [arXiv:hep-ph/0611027]; *J. Cosm. Astropart. Phys.* **0609**, 001 (2006) [arXiv:hep-ph/0605306].
- [35] M. Bolz, A. Brandenburg, W. Buchmuller, *Nucl. Phys.* **B606**, 518 (2001), Erratum *Nucl. Phys.* **B790**, 336 (2008) [arXiv:hep-ph/0012052].
- [36] J. Pradler, F.D. Steffen, *Phys. Rev.* **D75**, 023509 (2007) [arXiv:hep-ph/0608344].
- [37] J. Dunkley *et al.* [WMAP Collaboration], *Astrophys. J. Suppl.* **180**, 306 (2009) [arXiv:0803.0586[astro-ph]].
- [38] D.G. Cerdeno, Y. Mambrini, A. Romagnoni, *J. High Energy Phys.* **0911**, 113 (2009) [arXiv:0907.4985[hep-ph]].
- [39] R. Catena, P. Ullio, arXiv:0907.0018[astro-ph.CO].
- [40] J.F. Navarro, C.S. Frenk, S.D.M. White, *Astrophys. J.* **462**, 563 (1996) [arXiv:astro-ph/9508025]; J.F. Navarro, C.S. Frenk, S.D.M. White, *Astrophys. J.* **490**, 493 (1997) [arXiv:astro-ph/9611107].
- [41] B. Moore, S. Ghigna, F. Governato, G. Lake, T. Quinn, J. Stadel, P. Tozzi, *Astrophys. J.* **524**, L19 (1999).
- [42] F. Prada, A. Klypin, J. Flix, M. Martinez, E. Simonneau, *Phys. Rev. Lett.* **93**, 241301 (2004) [arXiv:astro-ph/0401512]; G. Bertone, D. Merritt, *Mod. Phys. Lett.* **A20**, 1021 (2005) [arXiv:astro-ph/0504422]; *Phys. Rev.* **D72**, 103502 (2005) [arXiv:astro-ph/0501555]; E. Athanassoula, F.S. Ling, E. Nezri, *Phys. Rev.* **D72**, 083503 (2005) [arXiv:astro-ph/0504631].
- [43] Y. Mambrini, C. Munoz, E. Nezri, F. Prada, *J. Cosm. Astropart. Phys.* **0601**, 010 (2006) [arXiv:hep-ph/0506204].
- [44] L. Bergstrom, J. Edsjo, P. Gondolo, P. Ullio, *Phys. Rev.* **D59**, 043506 (1999) [arXiv:astro-ph/9806072].
- [45] Y. Mambrini, *J. Cosm. Astropart. Phys.* **0912**, 005 (2009) [arXiv:0907.2918[hep-ph]]; E. Dudas, Y. Mambrini, S. Pokorski, A. Romagnoni, *J. High Energy Phys.* **0908**, 014 (2009) [arXiv:0904.1745[hep-ph]].
- [46] O. Adriani *et al.*, *Phys. Rev. Lett.* **102**, (2009) 051101 [arXiv:0810.4994[astro-ph]].

- [47] I.V. Moskalenko, A.W. Strong, J.F. Ormes, M.S. Potgieter, *Astrophys. J.* **565**, 280 (2002) [[arXiv:astro-ph/0106567](#)].
- [48] L.C. Tan, L.K. Ng, *J. Phys. G* **9**, 227, 1289 (1983).
- [49] J. Lavalle, Q. Yuan, D. Maurin, X.J. Bi, *Astron. Astrophys.* **479**, 427 (2008) [[arXiv:0709.3634\[astro-ph\]](#)].
- [50] J. Lavalle, J. Pochon, P. Salati, R. Taillet, *Astron. Astrophys.* **462**, 827 (2007) [[arXiv:astro-ph/0603796](#)].
- [51] V. Berezhinsky, V. Dokuchaev, Y. Eroshenko, *Phys. Rev.* **D68**, 103003 (2003) [[arXiv:astro-ph/0301551](#)].
- [52] D. Hooper, J.E. Taylor, J. Silk, *Phys. Rev.* **D69**, 103509 (2004) [[arXiv:hep-ph/0312076](#)].
- [53] T. Bringmann, P. Salati, *Phys. Rev.* **D75**, 083006 (2007) [[arXiv:astro-ph/0612514](#)].
- [54] D. Maurin, R. Taillet, C. Combet, [arXiv:astro-ph/0609522](#).
- [55] G. Bertone, A.R. Zentner, J. Silk, *Phys. Rev.* **D72**, 103517 (2005) [[arXiv:astro-ph/0509565](#)].
- [56] J. Diemand, B. Moore, J. Stadel, *Nature* **433**, 389 (2005) [[arXiv:astro-ph/0501589](#)].
- [57] T. Sjostrand, S. Mrenna, P. Skands, *J. High Energy Phys.* **0605**, 026 (2006) [[arXiv:hep-ph/0603175](#)].
- [58] M. Cirelli, A. Strumia, [[arXiv:0903.3381\[astro-ph\]](#)]
- [59] C. Goy [AMS Collaboration], *J. Phys. Conf. Ser.* **39**, 185 (2006).
- [60] T. Delahaye, R. Lineros, F. Donato, N. Fornengo, P. Salati, *Phys. Rev.* **D77**, 063527(2008) [[arXiv:0712.2312](#)]
- [61] A.W. Strong, I.V. Moskalenko, O. Reimer, *Astrophys. J.* **613**, 962 (2004) [[arXiv:astro-ph/0406254](#)]; E.A. Baltz, J. Edsjo, *Phys. Rev.* **D59**, 023511 (1998) [[arXiv:astro-ph/9808243](#)].
- [62] O. Adriani *et al.*, *Nature* **458**, 607 (2009) [[arXiv:0810.4995\[astro-ph\]](#)]
- [63] A.A. Abdo *et al.* [The Fermi LAT Collaboration], *Phys. Rev. Lett.* **102**, 181101 (2009) [[arXiv:0905.0025\[astro-ph.HE\]](#)].
- [64] A. Goudelis, Y. Mambrini, C. Yaguna, *J. Cosm. Astropart. Phys.* **0912**, 008 (2009) [[arXiv:0909.2799\[hep-ph\]](#)].
- [65] N. Bernal, A. Goudelis, Y. Mambrini, C. Munoz, *J. Cosm. Astropart. Phys.* **0901**, 046 (2009) [[arXiv:0804.1976\[hep-ph\]](#)].
- [66] L. Hernquist, *Astrophys. J.* **356**, 359 (1990).
- [67] S.H. Hansen, *Mon. Not. R. Astron. Soc.* **352**, L41 (2004) [[arXiv:astro-ph/0405371](#)].
- [68] G.R. Blumenthal, S.M. Faber, R. Flores, J.R. Primack, *Astrophys. J.* **301**, 27 (1986).
- [69] R. Jesseit, T. Naab, A. Burkert, *Astrophys. J. Lett.* **571**, L89 (2002) [[arXiv:astro-ph/0204164](#)].

- [70] O.Y. Gnedin, A.V. Kravtsov, A.A. Klypin, D. Nagai, *Astrophys. J.* **616**, 16 (2004) [[arXiv:astro-ph/0406247](#)].
- [71] J. Diemand, B. Moore, J. Stadel, *Mon. Not. R. Astron. Soc.* **353**, 624 (2004) [[arXiv:astro-ph/0402267](#)].
- [72] D. Merrit, *Phys. Rev. Lett.* **92**, 201304 (2004).
- [73] G. Bertone, D. Merritt, *Phys. Rev.* **D72**, 103502 (2005) [[arXiv:astro-ph/0501555](#)].
- [74] E. Athanassoula, F.S. Ling, E. Nezri, *Phys. Rev.* **D72**, 083503 (2005) [[arXiv:astro-ph/0504631](#)].